Letters

A Generic and Unified Global-Gyrator Model of Switched-Resonator Converters

Alon Cervera, *Student Member, IEEE*, Mor Mordechai Peretz, *Member, IEEE*, and Shmuel Ben-Yaakov, *Life Fellow, IEEE*

***Abstract*—A generic algebraic model of switched-resonator converters is developed and demonstrated by published and new converter configurations data. The model hinges on a newly introduced multiport global-gyrator matrix, of which the classical two-port gyrator is a private case. The main attribute of the skew-symmetrical as well as a Toeplitz global-gyrator matrix is that it expresses the magnitude and directions of the currents as a linear function of the port voltages with a constant gyration factor. The model is verified by previously published data, as well as new experimental and simulation results.**

***Index Terms*—DC-DC power conversion, gyrators, resonant power conversion, switched capacitor circuits, transfer function matrices.**

I. Introduction

SWITCHED-CAPACITOR converters (SCCs) have limited capabilities for voltage regulation due to the tight relationship between the voltage gain and the converter efficiency [1]–[10]. In such converters, the efficiency is equal to the ratio of the output voltage to the target voltage (the no-load SCC output voltage $V_{\rm target}$) $V_{\rm out}/V_{\rm target}$, which stems from the rigid proportionality between the input and output charges [1]–[10]. When loaded or controlled, the SCC output voltage will drop at the expense of internal losses due to parasitic resistances [6].

Regulation can be achieved either by varying the SCC parameters [1], [11], [12], by inserting a postregulation stage [13]–[15], or by generating multiple target voltages [1], [16]–[20]; but the system efficiency still remains of a discrete nature [21]–[24]. Resonant-type SCC (RSCC) has been employed [25]–[33] to reduce switching losses but since the operation of RSCCs is similar to the conventional SCCs in the sense that similar charge transfer applies, the efficiency of the converter is still strongly dependent on the voltage gain [9], [34]–[35]. That is, while the soft switching may reduce switching losses, the inherent rigid current transfer ratio remains, and the efficiency still follows the SCC relationship: $V_{\rm out}/V_{\rm target}$. Recent approaches to break the stiff relationship between efficiency and gain in SCC allow partial discharge of the capacitors back to the source [36]–[39] or combine resonant and linear operation deplete residual charge [40]–[42]. These two-port converters break the ground connection between input and output sides which limits the range of their practical application.

A recently developed gyrator behaved resonant-switched-capacitor converter (GRSCC) presented in [34], [43], and [44] disengages the efficiency of the SCC system from the voltage gain. The GRSCC exhibits a gyrator-like behavior [45]–[48] with continuous gain that can be controlled by pulse-density modulation (PDM) [49], [50]. These initial studies demonstrated that the GRSCC is capable of a variable gain operation without compromising the efficiency. This is achieved by introducing an additional switching state that provides an extra charge path to break the charge transfer ratio dictated by the precursor topology, and thereby vary the voltage transfer ratio without an efficiency penalty. The gyrator-like behavior in which the input and output currents are proportional to the output and input voltages, respectively, transforms the GRSCC into a voltage-dependent current source. This attribute is, by itself, an advantage in many power conversion applications, such as battery chargers and management systems, wide-bandwidth voltage regulation high-performance ICs, and high-intensity discharge lamps.

A pivotal advantage of the GRSCC as compared to the major previously described power gyrators is the fact that it possesses the capability of bidirectional power transfer. This is in contrast to the cases of a gyrator-like behavior with a unidirectional power delivery. This attribute could be extremely useful in a multitude of applications in which energy is temporary stored (one direction) and then delivered back (the other direction) as demonstrated in this letter. Nonetheless, the main benefit of the GRSCC is the ability to vary the gain by controlling the gyration factor which could be achieved, for example, by PDM [49], [50]. Since the GRSCCs operate under soft-switching conditions and can be realized using a single resonator, they are compatible with volume density demands.

One potential down side that is frequently argued with respect to modern converters' topologies, such as SCC or GRSCC, is the relatively large number of switches required for operation, which dictate switching sequences with higher complexity. However, recent microelectronics developments that make possible the fabrication of very low on resistance switches in

Manuscript received February 13, 2017; revised March 22, 2017; accepted April 10, 2017. Date of publication April 18, 2017; date of current version August 2, 2017. *(Corresponding author: Alon Cervera.)*

A. Cervera and M. M. Peretz are with the Center for Power Electronics and Mixed-Signal IC, Department of Electrical and Computer Engineering, Ben-Gurion University of the Negev, Beer-Sheva 8410501, Israel (e-mail: cervera@bgu.ac.il; morp@bgu.ac.il).

S. Ben-Yaakov is with the Department of Electrical and Computer Engineering, Ben-Gurion University of the Negev, Beer-Sheva 8410501, Israel (e-mail: sby@bgu.ac.il).

Color versions of one or more of the figures in this letter are available online at http://ieeexplore.ieee.org.

Digital Object Identifier 10.1109/TPEL.2017.2694858

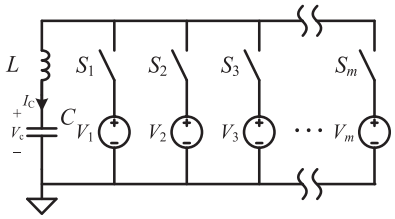

Fig. 1. Simplified model representation of a generic switched-resonator converter with *m* switched-source ports.

small packages seem to provide an ample answer to the "many switches" worry. A specific example that illustrates the integration feasibility and several attractive features of a GRSCC IC has been detailed in [51] as well as its application as a voltage regulator. Considering the many advantages of the GRSCC, it appears to be a viable candidate to be favored over the traditional switched-inductor converter topology in many applications. However, the theory that governs the operation of these converters and the potential topology variants that it could take are hitherto unknown. This letter unveils some of this terra incognita.

The objective of this letter is to develop a unified theory of the generic switched-resonator converter which includes any number of ports. This is accomplished by expressing the average currents of the generic structure of the converter as a recursive equation which leads to a unified and topology independent matrix that links the ports' currents to the voltages. The matrix has been found to be of the skew-symmetrical [52] and Toeplitz [53] form with some unique attributes that exhibit a multiport global-gyrator behavior.

II. Model Development

Without the loss of generality, consider the generic switched-resonator converter case as depicted in Fig. 1, which includes an *LC* resonator, *m* switches (S_i), and *m* ports of *m* voltage sources (V_i). The voltage sources represent power sources, loads (composed of a load equivalent resistor (R_L) in parallel to a filter capacitor (C_f)), or batteries that are charged or act as power sources. Internal resistances of the voltage sources and batteries and the equivalent series resistance (ESR) ofthe capacitors are neglected at this stage. It is further assumed that the losses of the resonant circuit, which is composed on the *LC* branch in series with the switch on resistance, are low, and, hence, the quality factor $Q \gg 1$ and the current waveform can be approximated by a sine waveform. Since the pulse duration is short, the relevant voltage terminals can be considered constant. To maintain zero current switching (ZCS), the on-time of each switch is $t_{\mathrm{on},i} = \pi\sqrt{LC}$. This assures ZCS at turn on and at turn off [34]. The total time for the system to complete a full cycle (i.e., repetition of *m* switching states t_{on}) is defined as *T*. Notice that *T* may be larger than $mt_{\mathrm{on},i}$ since dead time between the switching states $t_{\mathrm{on},i}$ is allowed. The analysis is done first for the case that the switches are turned on sequentially, one at a time, from $i = 1$ to *m* which is repeated perpetually.

Denoting the capacitor's voltage before the initiation of a switching state $t_{\mathrm{on},i}$, as $V_{C,i-1}$ and assuming high resonant quality factor and based on the behavior of a second-order circuit, the voltage $V_{C,i}$ at the end of the half-resonance switching point $t_{\mathrm{on},i}$ can be expressed as

$$V_{C,i} = V_{C,i-1} + 2\left(V_i - V_{C,i-1}\right) \tag{1a}$$

or

$$V_{C,i} = 2V_i - V_{C,i-1}. \tag{1b}$$

The charge ΔQ_i that is transferred from V_i to the capacitor *C* during a $t_{\mathrm{on},i}$ state is given by

$$\Delta Q_i = 2C\left(V_i - V_{C,i-1}\right) \tag{2}$$

and thus the average current of V_i (averaged over the full cycle *T*) can be expressed as

$$I_{\mathrm{av},i} = \frac{2C}{T}\left(V_i - V_{C,i-1}\right). \tag{3}$$

The capacitor voltage at the end of $t_{\mathrm{on},m}$, $V_{C,m}$ can now be expressed in a recursive fashion as

$$V_{C,m} = 2V_m - \left(2V_{m-1} - \left(2V_{m-2} \ldots - \left(2V_1 - V_{C,0}\right)\cdots\right)\right) \tag{4}$$

or

$$V_{C,m} = \sum_{i=1}^{m} 2V_i(-1)^{(i-1)} - V_{C,0}(-1)^{(m-1)}. \tag{5}$$

Assuming a stable operation, i.e., the capacitor voltage does not drift over time

$$V_{C,m} = V_{C,0}. \tag{6}$$

The theoretical implication of (5) depends on whether the sequence *m* is even or odd since it affects the sign of $V_{C,0}$ at the right side of the equality.

A. Odd Case

If *m* is odd, (5) implies

$$V_{C,m} = \sum_{i=1}^{m} 2V_i(-1)^{(i-1)} - V_{C,0} \tag{7}$$

from which

$$V_{C,0} = \sum_{i=1}^{m} V_i(-1)^{(i-1)}. \tag{8}$$

For algebraic reason, $V_{C,0}$ rather than $\mathrm{V_{C,m}}$ is placed on the left side of the equality. This form appears as noncausal, but in fact, since the operation is cyclic, (6) holds which implies that the capacitor voltage at the end of any $t_{\mathrm{on},i}$ is equal to the sum of the preceding *m* voltage sources. Applying (8) and considering the fact that the switching process is cyclic, the capacitor voltage prior to any switching state $t_{\mathrm{on},i}$ can be expressed as

$$V_{C,i-1} = \sum_{n=0}^{m-1} V_{i+n}(-1)^n. \tag{9}$$

In this expression, indexes larger than *m* are truncated to modulu (*m*).

Based on (3) and (9), the average current I_i for each switching state $t_{\mathrm{on},i}$ can be expressed as

$$I_i = \frac{2C}{T}\left[V_i - \sum_{n=0}^{m-1} V_{i+n}(-1)^n\right]. \tag{10}$$

Equation (10) can now be rewritten in a matrix form as follows:

$$\begin{bmatrix} I_1 \\ I_2 \\ I_3 \\ \vdots \\ I_m \end{bmatrix} = \frac{2C}{T}\begin{bmatrix} 0 & +1 & -1 & & -1 \\ -1 & 0 & +1 & \cdots & +1 \\ +1 & -1 & 0 & & -1 \\ & \vdots & & \ddots & \vdots \\ +1 & -1 & +1 & \cdots & 0 \end{bmatrix}\begin{bmatrix} V_1 \\ V_2 \\ V_3 \\ \vdots \\ V_m \end{bmatrix}. \tag{11}$$

Matrix (11) is a skew-symmetrical [52] as well as a Toeplitz [53] matrix of a unique form. It reveals that starting from a given $t_{\mathrm{on},i}$ that corresponds to a source V_i, the contribution of the following sources is alternating between positive and negative currents. That is, the odd or even position of a given source in the sequence determines whether it is a source or a load. It is interesting to note, although not surprising, that the sum of the I_{i} currents is zero. This is because *m* is odd and each row includes one zero. Consequently, the sum of each column is zero. The fact that the sum of the currents is zero is of course nothing but an expression of Kirchhoff's current law.

Matrix (11) introduces a new multiport global gyrator since it exhibits the basic nature of a gyrator: the current of each terminal voltage is a linear function–*with a constant gyration factor*–of all other terminal voltages.

The private case of $m = 3$ in which a voltage source V_1, a load V_2, and a short-circuit $V_3 = 0$ are switched in the sequence, can be represented as a 3×3 matrix (12). Here, the real rather than the normalized voltages are shown

$$\begin{bmatrix} I_1 \\ I_2 \\ I_3 \end{bmatrix} = \frac{2C}{T}\cdot\begin{bmatrix} 0 & +1 & -1 \\ -1 & 0 & +1 \\ +1 & -1 & 0 \end{bmatrix}\begin{bmatrix} V_1 \\ V_2 \\ 0 \end{bmatrix}. \tag{12}$$

From which

$$I_1 = \frac{2C}{T}V_2; \quad I_2 = -\frac{2C}{T}V_1. \tag{13}$$

Since the third column of (12) is multiplied by zero, V_1 and V_2 currents (I_1, I_2) can be expressed by the 2×2 matrix shown by the dashed boxes of (12) which is the familiar representation of the classical gyrator [45]–[48]. As already pointed out in [34], the switched-resonator converter that includes a source, a load, and short circuit exhibits the classical gyrator behavior with a gyration coefficient 2*C*/*T*.

Due to the unique nature of the global-gyrator matrix (11), the current direction can be reversed by changing the switching sequence from $\{V_1, V_2, 0\}$ to $\{V_2, V_1, 0\}$. Thus, bidirectional operation can be obtained by changing the switching sequence. Furthermore, since the multiport switched-resonator converter behaves as a gyrator, the voltage gains can be smaller or higher than one. Another feature is the ability to change the gyration coefficient by making the total cycle duration (*T*) longer than $mt_{\mathrm{on},i}$. That is, by introducing delays between switching states, the gyration coefficient is, in fact, controllable from the nominal values of 2*C*/*T* to lower values. Higher gains can also be achieved by repeated "visit" to a source. For example, using the same hardware, one can program the system to follow a sequence of five switching states $\{V_1, V_2, 0, V_2, 0\}$. The matrix representation for this case is

$$\begin{bmatrix} I_1 \\ I_2 \\ I_3 \\ I_4 \\ I_5 \end{bmatrix} = \frac{2C}{T}\begin{bmatrix} 0 & +1 & -1 & +1 & -1 \\ -1 & 0 & +1 & -1 & +1 \\ +1 & -1 & 0 & +1 & -1 \\ -1 & +1 & -1 & 0 & +1 \\ +1 & -1 & +1 & -1 & 0 \end{bmatrix}\begin{bmatrix} V_1 \\ V_2 \\ 0 \\ V_2 \\ 0 \end{bmatrix}. \tag{14}$$

From which

$$I(V_1) = \frac{4C}{T}V_2\,;\; I(V_2) = -\frac{4C}{T}V_1. \tag{15}$$

Hence, the gyration coefficient in this case is twice as large as compared to the basic coefficient (13).

It should be pointed out that the sources and/or loads could have either polarity, negative voltages can be accommodated as well. This, of course, affects the direction of the currents. For example, for a sequence of {–3 V, +5 V, 0} both of the currents are positive which means that the first voltage acts as a load while the second as a source.

B. Even Case

In the even case, (5) leads to

$$V_{C,m} = \sum_{i=1}^{m} 2V_i(-1)^{(i-1)} + V_{C,0}. \tag{16}$$

That is

$$\sum_{n=1}^{m} V_i(-1)^{i-1} = 0. \tag{17}$$

This relationship sets a severe constraint on the allowed values of sources V_i. If this relationship does not hold, then the system will be unstable due to the drift of the capacitor's voltage since the capacitor voltage at the end of the cycle V_{Cm} is not equal to the initial value $V_{C,0}$ at the beginning of the cycle. Nonetheless, as will be demonstrated in the next section, some switching schemes assure that (17) holds at all times regardless of the values of the voltages V_i and can, thus, be used successfully implemented.

C. Parasitic Resistances Effect

The global-gyrator model developed above assumes zero parasitic resistances. In reality, switch resistance, ESR of the capacitor, and the parasitic resistance of the inductor will deteriorate the performance. A thorough investigation of the parasitic effect in the topologies to be described below is beyond the scope of the letter. An initial investigation on this matter is presented in [54].

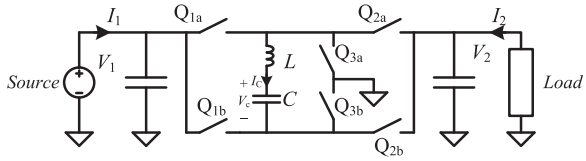

Fig. 2. Multimode switched-resonator converter.

III. Examples

Previous publications have described various basic topologies of the switched-resonant converter that includes three switching states [34], [43], [44], [55], [56]. These publications proved theoretically and experimentally that the basic three switching states topologies are gyrator-behaved-being a private case of the presented generic model. The examples below serve to illustrate the fitting of more elaborate switched-resonator topologies to the presented global-gyrator model.

A. Multimode Switched-Resonant Converter

The multimode switched-resonator converter of Fig. 2 can be controlled to realize seven resonator connections [54]. It is capable of executing odd and even numbers of switching states $t_{\mathrm{on},i}$. For example, the *odd* sequence $\{\mathrm{Q_{1a}}$ and $\mathrm{Q_{2b}}, \mathrm{Q_{2a}}$ and $\mathrm{Q_{3b}}$,and $\mathrm{Q_{3a}}$ and $\mathrm{Q_{2b}}\}$ produces the effective voltage sources $V_1 - V_2, V_2, -V_2$. Hence, the global-gyrator matrix is

$$\begin{bmatrix} I_1 \\ I_2 \\ I_3 \end{bmatrix} = \frac{2C}{T} \begin{bmatrix} 0 & +1 & -1 \\ -1 & 0 & +1 \\ +1 & -1 & 0 \end{bmatrix} \begin{bmatrix} V_1 - V_2 \\ V_2 \\ -V_2 \end{bmatrix}. \tag{18}$$

In this case, $I(V_1) = I_1, I(V_2) = I_2 - I_3$, which results in

$$I(V_1) = \frac{4C}{T} V_2 \; ; \; I(V_2) = -\frac{4C}{T} V_1 \tag{19}$$

exhibiting a gyration coefficient which is twice larger than the nominal one (13).The *even* sequence case $\{\mathrm{Q_{3a}}$and $\mathrm{Q_{2b}}$, $\mathrm{Q_{1a}}$ and $\mathrm{Q_{2b}}$, $\mathrm{Q_{2a}}$ and $\mathrm{Q_{3b}}$, and $\mathrm{Q_{2a}}$ and $\mathrm{Q_{1b}}\}$ entails the effective voltage sources $\{-V_2, V_1 - V_2, V_2, -V_1 + V_2, \}$. Even though the sequence is even, it produces a stable operation because the sum of all the effective voltage sources is zero independent on the values of V_1 and V_2. Hence, this sequence abides (17). This is demonstrated by the waveforms of Fig. 3 that have been obtained by an experimental system of Fig. 2 in which the essential parameters are: $V_1 = 5$ V, $V_2 = 1.2$ V, $C = 220$ nF, $L \approx 40$ nH, $t_{\mathrm{on}} = 300$ ns; the MOSFETs used where Siliconix SIA436DJ. The operation in this case is stable despite the severe limitation of (17).

The case of an even sequence when (17) is violated was examined by simulation. The results were found indicative of a divergence and pseudostabilization due to numerical truncation.

B. Voltage Gain Range Capabilities

The global-gyrator model predicts the possibility of realizing wide a voltage gain range by GRSCC. This has been demostarted by PSIM simulation of the sequence $\{V_{\mathrm{in}}, V_{\mathrm{out}}, 0\}$ for two cases:

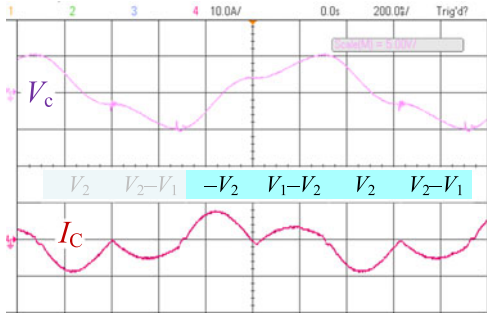

Fig. 3. Waveforms of the even case sequence: $\{-V_2, V_1 - V_2, V_2, -V_1 + V_2\}$ where (19) holds. Upper trace: Resonator capacitor voltage (5 V/div), lower trace: Resonator's current (10 A/div). Horizontal scale: 200 ns/div.

$V_{\mathrm{in}} = 5$ V, $V_{\mathrm{out}} = 20$ V and $V_{\mathrm{in}} = 20$ V, $V_{\mathrm{out}} = 5$ V. The simulation results (see Fig. 4) have been found to be in excellent agreement with model calculation, validating the model prediction of bidirectional operation. It is clear though that practical implementation of very large voltage gain may be hampered by unacceptable losses due to very high peak currents. This issue is beyond the scope of this letter.

C. DC Uninterruptible Power System (UPS)

The switched-resonator converter topology of Fig. 5 is used to demonstrate the flexibility of the generic global-gyrator model to cope with variable switching sequences. This topology can be conceived as a dc UPS system in which there is a primary voltage source V_{in} (which may be derived from the power line), a load represented by a resistor R, a filter capacitor C, and a battery V_{Bat}.

By programing the switching sequences, the UPS can be operated in three modes.

Mode 1: V_{in} is the main power source feeding the load and charging the battery.

Mode 2: V_{in} feeds the load, no battery charging.

Mode 3: V_{in} is absent, battery is powering the load.

The ports' voltages have been chosen as $V_{\mathrm{in}} = 5$ V; $V_{\mathrm{Load}} = 6$ V; and $V_{\mathrm{Bat}} = 4.5$ V. For the sake of brevity, only Mode 1 is discussed in this Letter in some detail.

Based on the alternate signs in each row of its global-gyrator matrix and the magnitude of the port voltages, it is observed that the sequence $\{S_1, S_2, S_3\}$ that produces the switching series $(V_{\mathrm{in}}, V_{\mathrm{Load}}, V_{\mathrm{Bat}})$ both feeds the load and charges the battery. This is clearly evident from the following matrix representation:

$$\begin{bmatrix} I_1 \\ I_2 \\ I_3 \end{bmatrix} = \frac{2C}{T_2} \begin{bmatrix} 0 & +V_L & -V_B \\ -V_{\mathrm{in}} & 0 & +V_B \\ +V_{\mathrm{in}} & -V_L & 0 \end{bmatrix}. \tag{20}$$

From which

$$\begin{cases} I(V_{\mathrm{in}}) = I_1 = \frac{2C}{T_2}(V_L - V_B) = \frac{2C}{T_2} \cdot 1.5 \\ I(V_L) = I_2 = \frac{2C}{T_2}(-V_{\mathrm{in}} + V_B) = -\frac{2C}{T_2} \cdot 0.5 \\ I(V_B) = I_3 = \frac{2C}{T_2}(V_{\mathrm{in}} - V_L) = -\frac{2C}{T_2} \cdot 1 \end{cases}. \tag{21}$$

This mode of operation has been tested by PSIM simulation with the following parameters: $C = 0.2$ μF; $L = 40$ nH;

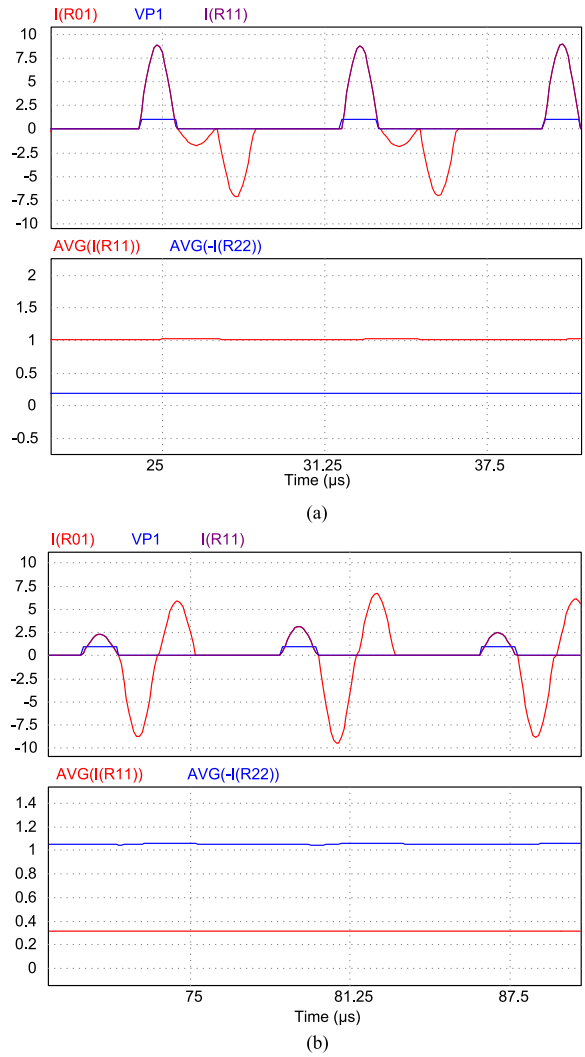

Fig. 4. PSIM simulation of the sequence: $\{V_{\rm in},\ V_{\rm out},0\}$ for two cases: (a) $V_{\rm in}=$ 5 V, $V_{\rm out}=$ 20 V. (b) $V_{\rm in}=$ 20 V and $V_{\rm out}=$ 5 V. Upper traces: Resonator current (0.5 A/div.) while the pulse indicates the switching duration of $V_{\rm in}$. Lower screens: Average currents for the voltage sources $V_{\rm in}$ and $V_{\rm out}$ (0.5 A/div.), higher current corresponds to the lower voltage.

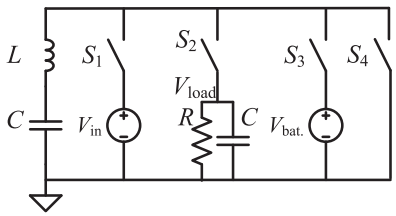

Fig. 5. Conceptual representation of a proposed switched-resonator UPS topology.

$f = 1/T = 850$ kHz. The simulation results (see Fig. 6) confirm the predicted mode of operation and the average currents are as calculated by (21). $I(V_{\rm in})$: Simulation 0.51 A, model calculated: 0.51 A; $I(V_{\rm L})$: Simulation 0.165A, model calculated 0.17A; $I(V_{\rm Bat})$: Simulation 0.342 A, model calculated: 0.34 A.

The above example demonstrates the up/down voltage gain and bidirectional current capabilities of the switched-resonator converter and the power of the global-gyrator model as a tool for synthesizing the switching sequences.

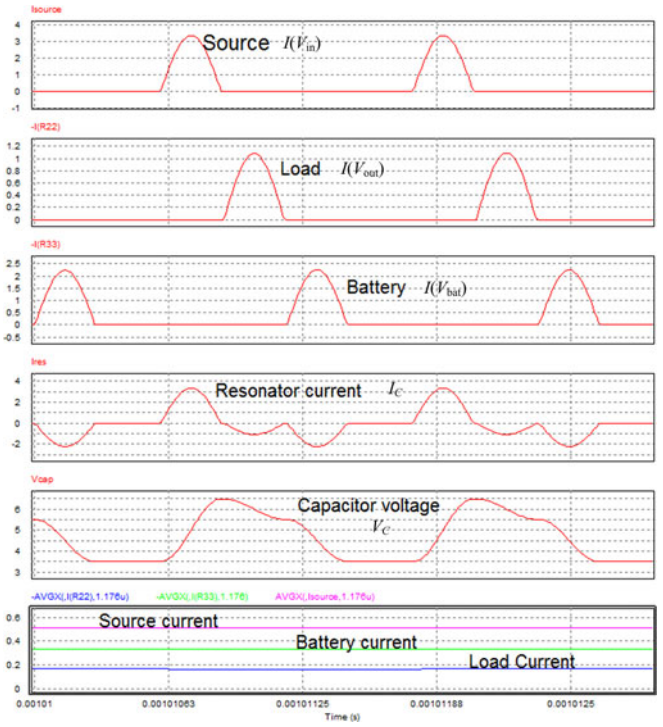

Fig. 6. Simulation results of the DC UPS. Traces: From up to down, $V_{\rm in}$ current, $V_{\rm load}$ current, $V_{\rm bat}$ current, resonator current, capacitor voltage. Lower screen, average currents for the voltage sources $V_{\rm in}$ (upper trace), $V_{\rm bat}$ (middle trace), $V_{\rm load}$ (lower trace).

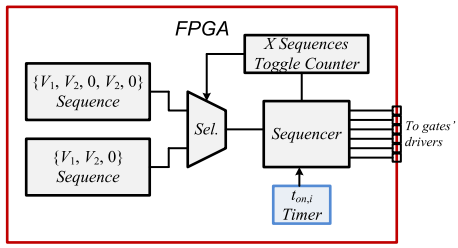

Fig. 7. Block diagram of the driving sequencer of the experiment.

D. Changing the Gyration Coefficient on the Fly

To further illustrate the predictive abilities of the global-gyrator model, we consider a switched-resonator system that includes three switches $\{S_1, S_2, S_3\}$ associated with three voltages $\{V_1, V_2, 0\}$. The system first follows the sequence V_1, V_2, 0 {which is the basic 2 × 2 gyrator case (12), and then programmed to follow the sequence $\{V_1, V_2, 0, V_2, 0\}$, with the controller realization is illustrated in Fig. 7. The latter is a five switching states sequence realized by repeated operation of same three switches $\{S_1, S_2, S_3\}$. This case corresponds to matrix (16) that yields a gyration factor of $4C/T_1$ as compared to $2C/T_2$ for the first switching sequence. It should be noted that for the fixed-switching state duration of the experiment, $T_2 = (5/3)T_1$. The essential waveforms of an experimental system that has been programmed to repeat the two sequences

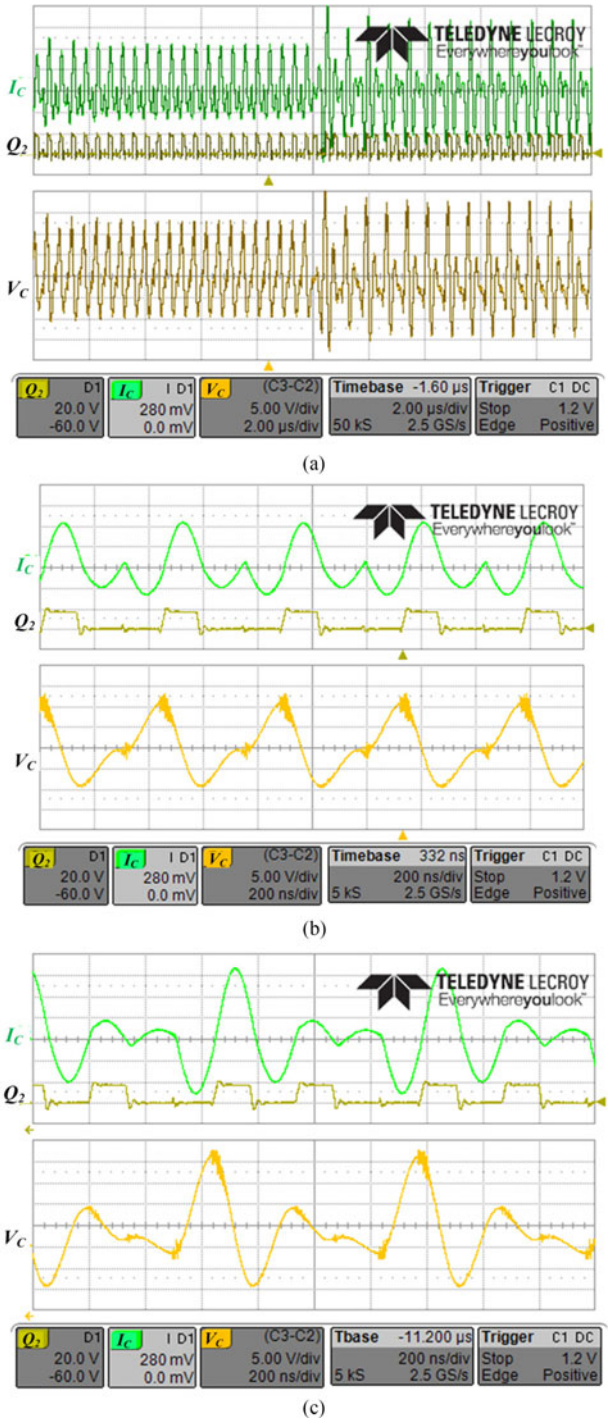

Fig. 8. Experimental results of the sequences V_1, V_2, 0 and $\{V_1, V_2, 0, V_2, 0\}$. In each screen, the upper trace is the resonator's current (relative scale) and the lower trace is the capacitor's voltage (5 V/div.). (a) Behavior when the two sequences are run in tandem. (b) Zoom on the three switching states case. (c) Zoom on the five switching states case.

in tandem are shown in Fig. 8. The basic data of the experimental system are as follows: $V_1 = 10$ V, $V_2 = 5$ V, $C = 33$ nF, $L \approx 75$ nH, $t_{\rm on} = 160$ ns; the MOSFETs used where Siliconix SIA466EDJ, driven by MAX17601 drivers. Control for the drive signals was obtained using FPGA (Altera Cyclone IV, DE-115).

The experimental results show a fast one cycle response of the switched-resonator converter upon a change from one mode to the other. The ratio of the experimental average currents of V_1 and V_2 has been found to be 1.45/1.65 A $= 0.878$, while the model prediction is (1/2)(3/5) $= 0.833$. The discrepancy is explained by the fact that the efficiencies for the two cases are different due to the differences in the rms currents. The efficiency for the three switching states case is measured to be 80%, while the efficiency for the five states is 77%. Correction of the experimental currents ratio by the efficiencies ratio $\{(0.878(77/80) = 0.845\}$ shows a very good agreement of the theoretically calculated values and the measured results.

IV. Conclusion

This letter investigated the behavior and potential of a multiport GRSCC. To this end, the multiport system has been analyzed and its core features have been extracted. The generic model of switched-resonator converters developed in this letter has been found to be of a global-gyrator form in which the current of each port is a linear function of the other switched voltages of the converter. The classical 2×2 gyrator matrix is found to be a private case of the global gyrator. This truncated gyrator is obtained where running a switched-resonator converter in a three switching states sequence, e.g., $\{V_1, V_2, 0)$. The model predicts stability for any odd switching sequences and for even switching sequences that obey (19).

The illustrative examples of this letter verify the features of the global gyrator matrix and highlight some of its potential to synthesize and analyze new GRSCC topologies. This letter verified the theoretical results regarding the different behavior of the odd and even cases by experiment and simulation. The bidirectionality and wide gain range of the GRSCC have been verified by simulation on a lossless converter with terminal voltages of 5 and 20 V. The flexibility of single multiterminal GRSCC to switch between operational functions has been demonstrated by considering a conceptual dc UPS in which a single four switch GRSCC fulfills the necessary tasks of feeding a load from a power source, charging a battery, and feeding the load from the battery. It is further verified experimentally that repeated switching sequences increases within one cycle, the gyration coefficient facilitating, thereby, a current boost. All the simulation and experimental results have been found to be in excellent agreement with the theoretical forecasts of the global-gyrator model.

As this letter concentrates on the generic features of the multiport and as such less emphasis is given on detailed design and analysis of a specific converters, or in-depth analysis of parasitic effects. Some of these have been introduced in an earlier study [54]. It is of interest to note that the GRSCC is compatible with the current quest for small size since the ZCS helps to reduce switching losses. Furthermore, the fact that the gyration ratio is equal to $2C/T$ implies that high frequency and large C enhance the GRSCC ability to deliver high power. The new global-gyrator model can be used to analyze switched-resonator converters, synthesis new configurations, and assess the advantages and limitations of alternative designs.

REFERENCES

[1] M. S. Makowski and D. Maksimovic, "Performance limits of switched-capacitor dc-dc converters," in *Proc. IEEE Power Electron. Spec. Conf.*, 1995, vol. 2, pp. 1215–1221.

[2] M. Budaes and L. Goras, "Burst mode switching mechanism for an inductorless dc-dc converter," in *Proc. CAS Int. Semicond. Conf.*, 2007, vol. 2, pp. 463–466.

[3] M. D. Seeman and S. R. Sanders, "Analysis and optimization of switched capacitor dc-dc converters," *IEEE Trans. Power Electron.*, vol. 23, no. 2, pp. 841–851, Mar. 2008.

[4] S. Ben-Yaakov and M. Evzelman, "Generic and unified model of switched capacitor converters," in *Proc. IEEE Energy Convers. Congr. Expo.*, 2009, pp. 3501–3508.

[5] J. M. Henry and J. W. Kimball, "Practical performance analysis of complex switched-capacitor converters," *IEEE Trans. Power Electron.*, vol. 26, no. 1, pp. 127–136, Jan. 2011.

[6] S. Ben-Yaakov, "On the influence of switch resistances on switched capacitor converters losses," *IEEE Trans. Ind. Electron. Lett.*, vol. 59, no. 1, pp. 638–640, Jan. 2012.

[7] J. M. Henry and J. W. Kimball, "Switched-capacitor converter state model generator," *IEEE Trans. Power Electron.*, vol. 27, no. 5, pp. 2415–2425, May 2012.

[8] P. K. Peter and V. Agarwal, "On the input resistance of a reconfigurable switched capacitor dc–dc converter-based maximum power point tracker of a photovoltaic source," *IEEE Trans. Power Electron.*, vol. 27, no. 12, pp. 4880–4893, Dec. 2012.

[9] M. Evzelman and S. Ben-Yaakov, "Average-current based conduction losses model of switched capacitor converters," *IEEE Trans. Power Electron.*, vol. 28, no. 7, pp. 3341–3352, Jul. 2013.

[10] B. Wu, L. Wang, L. Yang, K. Smedley, and S. Singer, "Comparative analysis of steady-state models for switched capacitor converter," *IEEE Trans. Power Electron.*, vol. 32, no. 2, pp. 1186–1197, Feb. 2017.

[11] H. S. H. Chung, "Development of DC/DC regulators based on switched-capacitor circuits," in *Proc. IEEE Int. Symp. Circuits Syst.*, 1999, vol. 5, pp. 210–213.

[12] M. Evzelman and R. Zane, "Burst mode control and switched-capacitor converters losses," in *Proc. IEEE Appl. Power Electron. Conf. Expo.*, 2016, pp. 1603–1607.

[13] S. Ben-Yaakov and A. Kushnerov, "Algebraic foundation of self adjusting switched capacitors converters," in *Proc. IEEE Energy Convers. Congr. Expo.*, 2009, pp. 1582–1589.

[14] R. C. N. Pilawa-Podgurski, D. M. Giuliano, and D. J. Perreault, "Merged two-stage power converter architecture with soft charging switched-capacitor energy transfer," in *Proc. IEEE Power Electron. Spec. Conf.*, 2008, pp. 4008–4015.

[15] S. Lim, J. Ranson, D. M. Otten, and D. J. Perreault, "Two-stage power conversion architecture for an LED driver circuit," in *Proc. IEEE Appl. Power Electron. Conf. Expo.*, 2013, pp. 854–861.

[16] Y. Beck and S. Singer, "Capacitive transposed series-parallel topology with fine tuning capabilities," *IEEE Trans. Circuits Syst. I, Reg. Papers*, vol. 58, no. 1, pp. 51–61, Jan. 2011.

[17] A. Kushnerov and S. Ben-Yaakov, "Unified algebraic synthesis of generalized Fibonacci switched capacitor converters," in *Proc. IEEE Energy Convers. Congr. Expo.*, 2012, pp. 774–778.

[18] Y. Beck, S. Singer, and L. M. Salamero, "Modular realization of capacitive converters based on general transposed series–parallel and derived topologies," *IEEE Trans. Ind. Electron.*, vol. 61, no. 3, pp. 1622–1631, Mar. 2014.

[19] L. G. Salem and P. P. Mercier, "A recursive switched-capacitor dc-dc converter achieving 2^{N-1} ratios with high efficiency over a wide output voltage range," *IEEE J. Solid-State Circuits*, vol. 49, no. 12, pp. 2773–2787, Dec. 2014.

[20] E. Hamo, A. Cervera, and M. M. Peretz, "Multiple conversion ratio resonant switched-capacitor converter with active zero current detection," *IEEE Trans. Power Electron.*, vol. 30, no. 4, pp. 2073–2083, Apr. 2015.

[21] G. Zhu and A. Ioinovici, "Switched-capacitor power supplies: DC voltage ratio, efficiency, ripple, regulation," in *Proc. IEEE Int. Symp. Circuits Syst.*, Atlanta, GA, USA, 1996, pp. 553–556.

[22] H. S. Chung, A. Ioinovici, and Wai-Leung Cheung, "Generalized structure of bi-directional switched-capacitor DC/DC converters," *IEEE Trans. Circuits Syst. I, Fundam. Theory Appl.*, vol. 50, no. 6, pp. 743–753, Jun. 2003.

[23] M. D. Seeman, V. W. Ng, H. P. Le, M. John, E. Alon, and S. R. Sanders, "A comparative analysis of switched-capacitor and inductor-based dc-dc conversion technologies," in *Proc. IEEE Workshop Control Modeling Power Electron.*, 2010, pp. 1–7.

[24] Y. Lei and R. C. N. Pilawa-Podgurski, "A general method for analyzing resonant and soft-charging operation of switched-capacitor converters," *IEEE Trans. Power Electron.*, vol. 30, no. 10, pp. 5650–5664, Oct. 2015.

[25] Y.-S. Lee, Y.-Y. Chiu, and M.-W. Cheng, "ZCS switched-capacitor bi-directional quasi-resonant converters," in *Proc. IEEE Int. Conf. Power Electron. Drive Syst.*, 2005, pp. 866–871.

[26] Y.-S. Lee and Y.-P. Ko, "Switched-capacitor bi-directional converter performance comparison with and without quasi-resonant zero-current switching," *IET Power Electron.*, vol. 3, no. 2, pp. 269–278, Mar. 2010.

[27] M. Shoyama, T. Naka, and T. Ninomiya, "Resonant switched-capacitor converter with high efficiency," in *Proc. IEEE Power Electron. Spec. Conf.*, 2004, vol. 5, pp. 3780–3786.

[28] Y. P. B. Yeung, K. W. E. Cheng, S. L. Ho, K. K. Law, and D. Sutanto, "Unified analysis of switched-capacitor resonant converters," *IEEE Trans. Ind. Electron.*, vol. 51, no. 4, pp. 864–873, Aug. 2004.

[29] A. Ioinovici, H. S. H. Chung, M. S. Makowski, and C. K. Tse, "Comments on 'unified analysis of switched-capacitor resonant converters'," *IEEE Trans. Ind. Electron.*, vol. 54, no. 1, pp. 684–685, Feb. 2007.

[30] O. Keiser, P. K. Steimer, and J. W. Kolar, "High power resonant switched-capacitor step-down converter," in *Proc. IEEE Power Electron. Spec. Conf.*, 2008, pp. 2772–2777.

[31] D. Cao and F. Z. Peng, "Multiphase multilevel modular dc–dc converter for high-current high-gain TEG application," *IEEE Trans. Ind. Appl.*, vol. 47, no. 3, pp. 1400–1408, May/Jun. 2011.

[32] D. Cao and F. Z. Peng, "Zero-current-switching multilevel modular switched-capacitor dc–dc converter," *IEEE Trans. Ind. Appl.*, vol. 46, no. 6, pp. 2536–2544, Nov./Dec. 2010.

[33] D. Cao, S. Jiang, and F. Z. Peng, "Optimal design of multilevel modular switched-capacitor dc-dc converter," in *Proc. IEEE Energy Convers. Congr. Expo.*, 2011, pp. 537–544.

[34] A. Cervera, M. Evzelman, M. M. Peretz, and S. Ben-Yaakov, "A high efficiency resonant switched capacitor converter with continuous conversion ratio," *IEEE Trans. Power Electron.*, vol. 30, no. 3, pp. 1373–1382, Mar. 2015.

[35] R. Beiranvand, "Analysis of a switched-capacitor converter above its resonant frequency to overcome voltage regulation issue of resonant SCCs," *IEEE Trans. Ind. Electron.*, vol. 63, no. 9, pp. 5315–5325, Sep. 2016.

[36] D. Qiu and B. Zhang, "Analysis of step-down resonant switched capacitor converter with sneak circuit state," in *Proc. IEEE Power Electron. Spec. Conf.*, 2006, pp. 1–5.

[37] W. Tu, D. Qiu, B. Zhang, and J. Li, "Sneak circuit analysis in n-stage resonant switched capacitor converters," in *Proc. Int. Workshop Anti-Counterfeiting, Secur. Identification*, 2007, pp. 61–65.

[38] W. Tu, D. Qiu, B. Zhang, and J. Li, "General laws of sneak circuit in resonant switched capacitor converters," in *Proc. IEEE Power Electron. Spec. Conf.*, 2007, pp. 708–712.

[39] Y. Ye, K. W. E. Cheng, J. Liu, and C. Xu, "A family of dual-phase-combined zero-current switching switched-capacitor converters," *IEEE Trans. Power Electron.*, vol. 29, no. 8, pp. 4209–4218, Aug. 2014.

[40] K.-H. Liu, R. Oruganti, and F. C. Lee, "Resonant switches—Topologies and characteristics," in *Proc. IEEE Power Electron. Spec. Conf.*, 1985, pp. 106–116.

[41] M. Jabbari, "Unified analysis of switched-resonator converters," *IEEE Trans. Power Electron.*, vol. 26, no. 5, pp. 1364–1376, May 2011.

[42] S. Sharifi and M. Jabbari, "Family of single-switch quasi-resonant converters with reduced inductor size," *IET Power Electron.*, vol. 7, no. 10, pp. 2544–2554, 2014.

[43] A. Cervera and M. M. Peretz, "Resonant switched-capacitor voltage regulator with ideal transient response," *IEEE Trans. Power Electron.*, vol. 30, no. 9, pp. 4943–4951, Sep. 2015.

[44] A. Cervera and M. M. Peretz, "Envelope tracking power supply for volume-sensitive low-power applications based on a resonant switched-capacitor converter," in *Proc. IEEE Appl. Power Electron. Conf. Expo.*, 2016, pp. 2298–2303.

[45] B. D. Tellegen, "The gyrator, a new electric network element," *Philips Res. Rep.*, vol. 3, no. 2, pp. 81–101, 1948.

[46] S. Singer, "Gyrators application in power processing circuits," *IEEE Trans. Ind. Electron.*, vol. IE-34, no. 3, pp. 313–318, Aug. 1987.

[47] G. Pillonnet, "Modeling and efficiency analysis of multiphase resonant-switched capacitive converters," *IEEE Trans. Power Electron.*, vol. 31, no. 1, pp. 11–14, Jan. 2016.

[48] D. Shmilovitz, "Gyrator realization based on a capacitive switched cell," *IEEE Trans. Circuits Syst. II, Exp. Briefs*, vol. 53, no. 12, pp. 1418–1422, Dec. 2006.

[49] Y.-H. Liu, S.-C. Wang, and Y.-F. Luo, "Digital dimming control of CCFL drive system using pulse density modulation technique," in *Proc. IEEE Region 10 Conf.*, 2007, pp. 1–4.

[50] X. Zhang *et al.*, "A 1-V-input switched-capacitor voltage converter with voltage-reference-free pulse-density modulation," *IEEE Trans. Circuits Syst. II, Exp. Briefs*, vol. 59, no. 6, pp. 361–365, Jun. 2012.

[51] E. Abramov, A. Cervera, and M. M. Peretz, "Optimal design of a voltage regulator based resonant switched-capacitor converter IC," in *Proc. IEEE Appl. Power Electron. Conf.*, 2016, pp. 692–699.

[52] H. D. Luke and H. D. Schotten, "Odd-perfect, almost binary correlation sequences," *IEEE Trans. Aerosp. Electron. Syst.*, vol. 31, no. 1, pp. 495–498, Jan. 1995.

[53] K. B. Petersen and M. S. Pedersen, *The Matrix Cookbook*. Kgs. Lyngby, Denmark: Technical Univ. Denmark, 2012.

[54] A. Cervera, S. Ben-Yaakov, and M. M. Peretz, "Single-stage switched-resonator converter topology with wide conversion ratio for volume sensitive applications," in *Proc. IEEE Appl. Power Electron. Conf. Expo.*, 2017, pp. 1706–1712.

[55] A. Cervera and M. M. Peretz, "Envelope tracking power supply for volume-sensitive low-power applications based on a resonant switched-capacitor converter," in *Proc. IEEE Appl. Power Electron. Conf. Expo.*, 2016, pp. 2298–2303.

[56] O. Kirshenboim, A. Cervera, and M. M. Peretz, "Improving loading and unloading transient response of a voltage regulator module using a load-side auxiliary gyrator circuit," *IEEE Trans. Power Electron.*, vol. 32, no. 3, pp. 1996–2007, Mar. 2017.